



HAL
open science

The autophagy protein ATG16L1 cooperates with IFT20 and INPP5E to regulate the turnover of phosphoinositides at the primary cilium

Asma Boukhalifa, Federica Roccio, Nicolas Dupont, Patrice Codogno, Etienne Morel

► To cite this version:

Asma Boukhalifa, Federica Roccio, Nicolas Dupont, Patrice Codogno, Etienne Morel. The autophagy protein ATG16L1 cooperates with IFT20 and INPP5E to regulate the turnover of phosphoinositides at the primary cilium. *Cell Reports*, 2021, 35 (4), pp.109045. 10.1016/j.celrep.2021.109045 . hal-03246943

HAL Id: hal-03246943

<https://u-paris.hal.science/hal-03246943v1>

Submitted on 2 Jun 2021

HAL is a multi-disciplinary open access archive for the deposit and dissemination of scientific research documents, whether they are published or not. The documents may come from teaching and research institutions in France or abroad, or from public or private research centers.

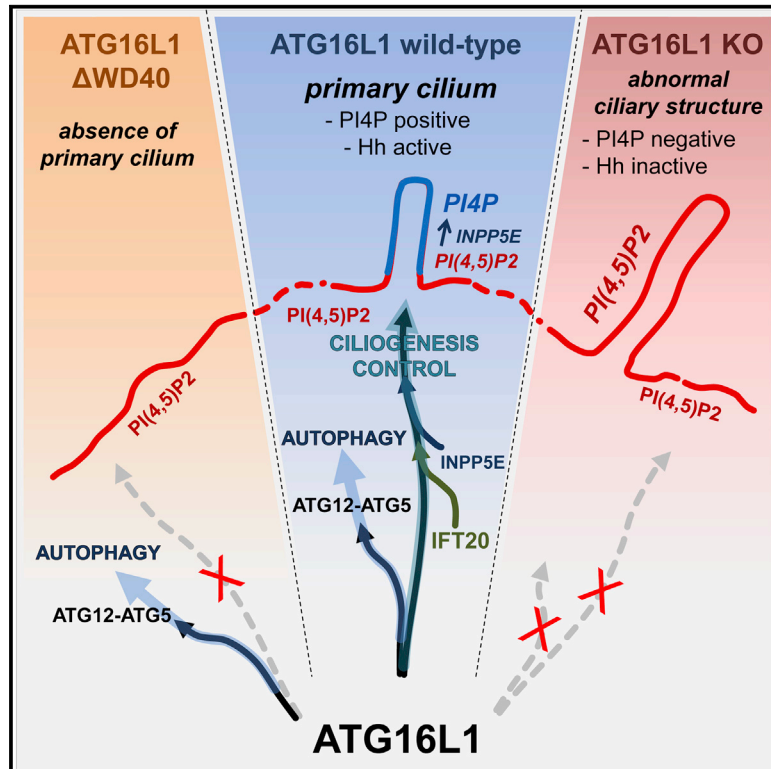
L'archive ouverte pluridisciplinaire **HAL**, est destinée au dépôt et à la diffusion de documents scientifiques de niveau recherche, publiés ou non, émanant des établissements d'enseignement et de recherche français ou étrangers, des laboratoires publics ou privés.



Distributed under a Creative Commons Attribution 4.0 International License

The autophagy protein ATG16L1 cooperates with IFT20 and INPP5E to regulate the turnover of phosphoinositides at the primary cilium

Graphical abstract



Authors

Asma Boukhalifa, Federica Roccio, Nicolas Dupont, Patrice Codogno, Etienne Morel

Correspondence

patrice.codogno@inserm.fr (P.C.),
etienne.morel@inserm.fr (E.M.)

In brief

Boukhalifa et al. report a non-canonical role for autophagy protein ATG16L1 during primary cilium biogenesis. ATG16L1 interacts with IFT20 and INPP5E to regulate elongation of the primary cilium and primary-cilium-dependent signaling. Deletion of the WD40 domain of ATG16L1 impairs ciliogenesis but not autophagy.

Highlights

- ATG16L1 regulates ciliogenesis independently of macroautophagy
- ATG16L1 interacts with ciliary protein IFT20 via WD40 domain to regulate ciliogenesis
- ATG16L1 interacts with the phosphoinositide-associated phosphatase INPP5E
- Loss of ATG16L1 interaction with INPP5E leads to a default of PI4P at the primary cilium



Article

The autophagy protein ATG16L1 cooperates with IFT20 and INPP5E to regulate the turnover of phosphoinositides at the primary cilium

Asma Boukhalfa,^{1,2} Federica Roccio,¹ Nicolas Dupont,¹ Patrice Codogno,^{1,*} and Etienne Morel^{1,3,*}¹Institut Necker-Enfants Malades (INEM), INSERM U1151-CNRS UMR 8253, Université de Paris, Paris, France²Present address: Molecular Cardiology Research Institute, Tufts Medical Center, Boston, MA, USA³Lead contact*Correspondence: patrice.codogno@inserm.fr (P.C.), etienne.morel@inserm.fr (E.M.)<https://doi.org/10.1016/j.celrep.2021.109045>

SUMMARY

The primary cilium (PC) regulates signalization linked to external stress sensing. Previous works established a functional interplay between the PC and the autophagic machinery. When ciliogenesis is promoted by serum deprivation, the autophagy protein ATG16L1 and the ciliary protein IFT20 are co-transported to the PC. Here, we demonstrate that IFT20 and ATG16L1 are part of the same complex requiring the WD40 domain of ATG16L1 and a Y-E-F-I motif in IFT20. We show that ATG16L1-deficient cells exhibit aberrant ciliary structures, which accumulate PI4,5P₂, whereas PI4P, a lipid normally concentrated in the PC, is absent. Finally, we demonstrate that INPP5E, a phosphoinositide-associated phosphatase responsible for PI4P generation, interacts with ATG16L1 and that a perturbation of the ATG16L1/IFT20 complex alters its trafficking to the PC. Altogether, our results reveal a function of ATG16L1 in ciliary lipid and protein trafficking, thus directly contributing to proper PC dynamics and functions.

INTRODUCTION

The primary cilium (PC) is a microtubule-based antenna present at the surface of many cell types. It serves as an environmental sensor to integrate chemical (such as hormones and nutrients), morphogens, and physical (mucus flow and fluid flow) stimuli (Goetz and Anderson, 2010; Satir et al., 2010; Malicki and Johnson, 2017; Nachury and Mick, 2019). The PC is organized into three substructures: the basal body that matures from the mother centriole, the axoneme that protrudes from the cell surface, and the transitory zone that allows proteins to be transported into the axoneme from the cytosol (Satir et al., 2010). PC dynamics is closely linked to cell cycle progression, it assembles in cells exiting the cell cycle and disassembles when cells enter the cell cycle (Izawa et al., 2015; Wang and Dynlacht, 2018). Ciliogenesis depends on intraflagellar transport (IFT) particles (Goetz and Anderson, 2010; Satir et al., 2010; Malicki and Johnson, 2017; Nachury and Mick, 2019). Intraflagellar transport complex B (IFTB), a complex composed of 14 proteins, transports cargoes to the tip of the axoneme in a kinesin-2-dependent manner, whereas IFTA, composed of 6 proteins, transports cargo from the tip of the axoneme to the cytoplasm in a dynein-2-dependent manner (He et al., 2017). Defective PC function is the cause of many human diseases known as ciliopathies. These diseases can target several organs and mostly lead to developmental disorders (Braun and Hildebrandt, 2017; Reiter and Leroux, 2017).

Recent studies illuminate the crosstalk between PC and macroautophagy (hereafter, referred to as autophagy), a major lysosomal

degradative pathway for intracellular material (Boya et al., 2013; Bento et al., 2016; Levine and Kroemer, 2019). PC-dependent autophagy is activated by different stimuli, including growth factors, nutrient deprivation (Pampliega et al., 2013; Tang et al., 2013), and mechanical stress (Orhon et al., 2016; Xiang et al., 2019; Zemirli et al., 2019; Boukhalfa et al., 2020; Miceli et al., 2020). Reciprocally, many studies showed that autophagy is able to control PC length and dynamics (Pampliega et al., 2013; Orhon et al., 2015; Cao and Zhong, 2016; Boukhalfa et al., 2019; Morleo and Franco, 2019; Zemirli et al., 2019). Autophagy has been shown to control the turnover of ciliary proteins, including IFT20 and OFD1 (Lam et al., 2013; Pampliega et al., 2013; Tang et al., 2013) and the term “ciliophagy” has been proposed for the degradation of ciliary proteins by autophagy (Cloonan et al., 2014). However, further studies need to clarify the role of the autophagic machinery in the regulation of ciliogenesis and in the selectivity of ciliary-protein degradation.

During the induction of PC-dependent autophagic pathway, most of the autophagy-related (ATG) proteins engaged in the autophagosome formation to sequester cytosolic cargo are recruited at the vicinity of the PC (Pampliega et al., 2013). Notably ATG16L1, a key protein in the regulation of the autophagy sequence (Fujita et al., 2008), has been shown to accumulate at the basal body and in the axoneme (Pampliega et al., 2013; Orhon et al., 2016). Moreover, ATG16L1 is present with the ciliary protein IFT20 in the same vesicular compartment en route to the primary cilium and the deletion of IFT20 protein alters the formation of autophagosomes (Pampliega et al., 2013).



In the present work, we functionally document the previously reported ATG16L1-IFT20 interaction (Pampliega et al., 2013), and we report that ATG16L1 dialogs with the phosphoinositide phosphatase INPP5E, which is associated with the Joubert syndrome, a recessive neurodevelopmental ciliopathy (Bielas et al., 2009). INPP5E hydrolyzes PI(4,5)P₂ to produce PI4P, whose homeostasis at PC is a key feature of ciliary identity (Xu et al., 2016). PI4P is also required in the membrane of the axoneme for a proper trafficking of PC-associated signaling proteins (Chávez et al., 2015; Garcia-Gonzalo et al., 2015).

We show that ATG16L1 is a PI4P-interacting protein and that, in the absence of ATG16L1, PI(4,5)P₂ accumulates at the expense of PI4P and affects ciliogenesis by altering PC organization and signaling functions, leading to a giant cilium-like structure. We show that the proper trafficking of INPP5E is dependent on the interaction between ATG16L1 and IFT20.

We show that ATG16L1 and IFT20 molecular dialog is mediated by a specific motif, previously identified in TMEM59B protein (Boada-Romero et al., 2013), which is present in IFT20 and by the WD40 domain of ATG16L1, known to be dispensable for canonical autophagy (Fletcher et al., 2018). We deepened these findings by demonstrating that the function of ATG16L1 in IFT20 and INPP5E crosstalk is independent of its role in canonical autophagy.

In conclusion, our study uncovers a function for ATG16L1 in ciliary trafficking and PC membrane turnover beyond its role in autophagy, underlining the intricate relation between the autophagic and the ciliary machineries.

RESULTS

IFT20 and ATG16L1 are part of the same complex from Golgi to primary cilium

To study the interplay of IFT20 and ATG16L1 in the context of ciliogenesis, we analyzed their behavior during serum-deprivation-induced ciliogenesis in mouse embryonic fibroblasts (MEFs), as previously described (Pampliega et al., 2013). In the full-medium culture condition, IFT20 is mostly associated with the Golgi apparatus and the centrosome (Figure 1A; serum condition) (Follit et al., 2006, 2008; Pampliega et al., 2013). Under serum deprivation, IFT20 is transported to the PC, as confirmed by axoneme co-staining with the ciliary protein ARL13B (Figure 1A, minus serum condition). PC-associated IFT20 is mostly present at the axoneme (Figures 1B and 3D, acquisition). This peculiar localization is only detected with a methanol-based fixation (which is not compatible with some other antigens), because classical paraformaldehyde fixation does not allow the proper detection of the axonemal pool of IFT20 (Figure 1C). Stimulation of autophagy is also a hallmark of serum deprivation, as shown here by the increase in the LC3-II level (Figures 1D and 1E) and by the accumulation of LC3 and ATG13 puncta (Figures S1A and S1B). In the absence of serum, we also observed an accumulation of total cellular IFT20 (Figures 1D and 1E), as previously reported (Pampliega et al., 2013). Remarkably, the centrosomal and Golgi localization of IFT20 in MEFs cultured in complete medium is similar to that observed in non-ciliated cells, such as HepG2 cells (De La Iglesia and Porta, 1967; Wheatley, 1969) (Figure 1G).

IFT20, which interacts with the Golgi protein GMAP210 (Follit et al., 2008), is essential for ciliogenesis and Golgi-ciliary trafficking (Follit et al., 2006). Accordingly, *ift20*^{-/-} MEF cells (Figure S2A) are not able to protrude a ciliary structure in the absence of serum (Figures S2B and S2C).

Previous data report a co-distribution of IFT20 with the autophagy protein ATG16L1 (Pampliega et al., 2013). In MEFs cultured in the presence of serum (thus non-ciliated), perinuclear pools of ATG16L1 and IFT20 co-distribute (Figure 2A), whereas, in the absence of serum, ATG16L1 and IFT20 co-localize at the PC (Figure 2B).

This suggests that IFT20 and ATG16L1 might interact. To test that hypothesis, we first performed pull-down experiments using purified human ATG16L1^{GST} recombinant protein as bait. Under those conditions, we were able to pull down recombinant IFT20 protein in an *in vitro* assay (Figure 2C). To test the interaction in living cells, we used ATG16L1 and IFT20 knockout/rescued cells expressing ATG16L1^{GFP} and/or IFT20^{mCherry}. Re-expression of the fluorescent-tagged version of ATG16L1 and IFT20 in knockdown cells allows a balanced ratio of proteins because overexpression of ATG16L1 leads to alteration of biological functions, probably because it induces deregulation of ATG16L1-containing complexes (Fujita et al., 2008). This was observed in wild-type MEFs transfected with ATG16L1^{GFP}, in which GFP-positive puncta were detected at subcellular localizations negative for endogenous ATG16L1 (Figure S3A) (Li et al., 2017). Moreover, ATG16L1^{GFP} was not detected at the PC positive for the endogenous protein (Figure S3B). The experimental setup (i.e., *ift20*^{-/-} MEFs transfected with IFT20^{mCherry}, and *Atg16L1*^{-/-} MEFs transfected with ATG16L1^{GFP}) allowed GFP and mCherry-driven co-immunoprecipitation. This confirmed that IFT20 and ATG16L1 can be found in the same complex in the presence of serum (Figures S4A and S4B) and in the absence of serum (Figures 2D and S4C), as previously suggested (Pampliega et al., 2013).

ATG16L1 is a central protein in the initiation of autophagosome biogenesis, its main function is dedicated to LC3 lipidation/targeting to autophagosomal membrane and requires its association with ATG5 and ATG12 (Fujita et al., 2008). To investigate whether IFT20 association with ATG16L1 depended on the autophagy machinery, we tested the ability of endogenous ATG16L1 to immunoprecipitate endogenous IFT20 using anti-ATG16L1 antibodies in MEFs knockout for *Atg3*, a key regulator of LC3 lipidation (Tanida et al., 2006) and in MEF knockout for *Atg5*. IFT20 and ATG16L1 still co-immunoprecipitated in the absence of either ATG3 or ATG5 (Figure 2E). These results strongly suggest that the interaction of ATG16L1 with IFT20 is not dependent on the classical autophagic machinery. We, furthermore, investigated whether other key proteins of the initiation of autophagosome formation were present in the IFT20/ATG16L1 complex. Both Vps34 and Beclin1, responsible for local synthesis of PI3P at the autophagosomal membrane (Nascimbeni et al., 2017), did not co-immunoprecipitate with ATG16L1, hinting that they are not part of the IFT20/ATG16L1 complex (Figure S4D). Taken together, these results suggest that ATG16L1, in a complex with IFT20, has a non-canonical role during ciliogenesis.

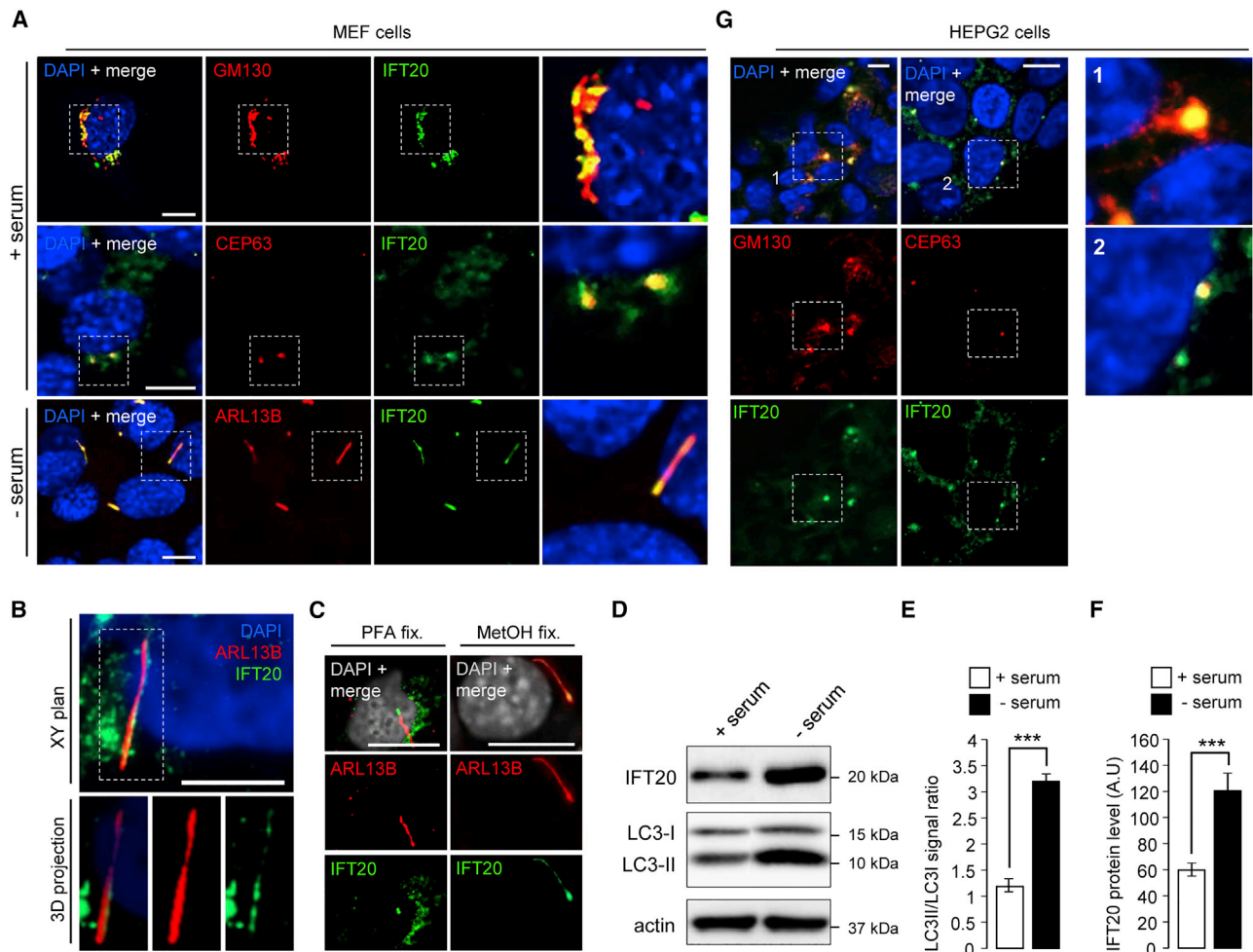


Figure 1. IFT20 subcellular localization and ciliogenesis status

(A) Confocal analysis of MEF cells cultured in presence (+ serum) or 24-h absence of serum (– serum) and processed for immunofluorescence using DAPI, anti-IFT20, anti-GM130 (Golgi marker), anti-CEP63 (centrosomal marker), and anti-ARL13B (a primary cilium [PC] marker.). Scale bar: 10 μ m

(B) Three-dimensional (3D) confocal acquisition of MEF cells cultured for 24 h in the absence of serum and processed for immunofluorescence using DAPI, anti-IFT20, and anti-ARL13B. Scale bar: 5 μ m.

(C) Comparison of IFT20 subcellular pattern, using DAPI, anti-IFT20, and anti-ARL13B antibodies, in MEF cells cultured for 24 h in the absence of serum and fixed with paraformaldehyde (PFA) or cold methanol (MeOH), showing IFT20 at the base of the PC in PFA fixation and IFT20 in the PC axoneme in MeOH fixation. Scale bar: 5 μ m.

(D) MEF cells were cultured in presence (+ serum) or 24 h absence of serum (– serum) and processed for analysis by SDS-PAGE and western blotting using anti-IFT20, anti-LC3, and anti-actin antibodies.

(E) Bar diagram showing the quantification of LC3II/LC3I ratio levels shown in (D) in the presence (+ serum) or in the absence (– serum) of serum.

(F) Bar diagram showing the quantification of relative IFT20 levels shown in (D) in the presence (+ serum) or in the absence (– serum) of serum. AU, arbitrary units.

(G) Confocal analysis of HEPG2 cells processed for immunofluorescence using DAPI, anti-IFT20, anti-GM130 (Golgi marker, right panel), and anti-CEP63 (centrosomal marker, right panel). Scale bars: 10 μ m.

Values in (E) and (F) denote means \pm SD (n = 3 independent experiments). ***p < 0.001 using the Student's t test.

Exocyst component Sec8 is a partner of ATG16L1 and IFT20 during ciliogenesis

IFT20 was recently reported to be associated with subunits of the exocyst complex, whose function is directly connected to post-Golgi trafficking (Fogelgren et al., 2011; Nachury et al., 2010; Wu and Guo, 2015; Monis, Faundez and Pazour, 2017). The exocyst is also associated with both autophagy regulation (Joffre et al., 2015; Nishida-Fukuda, 2019) and PC turnover (Nachury et al.,

2010). Here, using co-immunoprecipitation technique, we show that the exocyst Sec8 protein interacts with IFT20, but only in ciliated (i.e., serum-deprived) cells (Figure S5A). Small interfering RNA (siRNA)-mediated knockdown of Sec8 led to exocyst destabilization (as assessed by SEC10 levels; Figure S5B), ciliogenesis abrogation, and IFT20 relocalization on intracellular structures (Figure S5C), which were mostly identified as Golgi membranes (Figure S5D). Altogether, these data demonstrate that ATG16L1

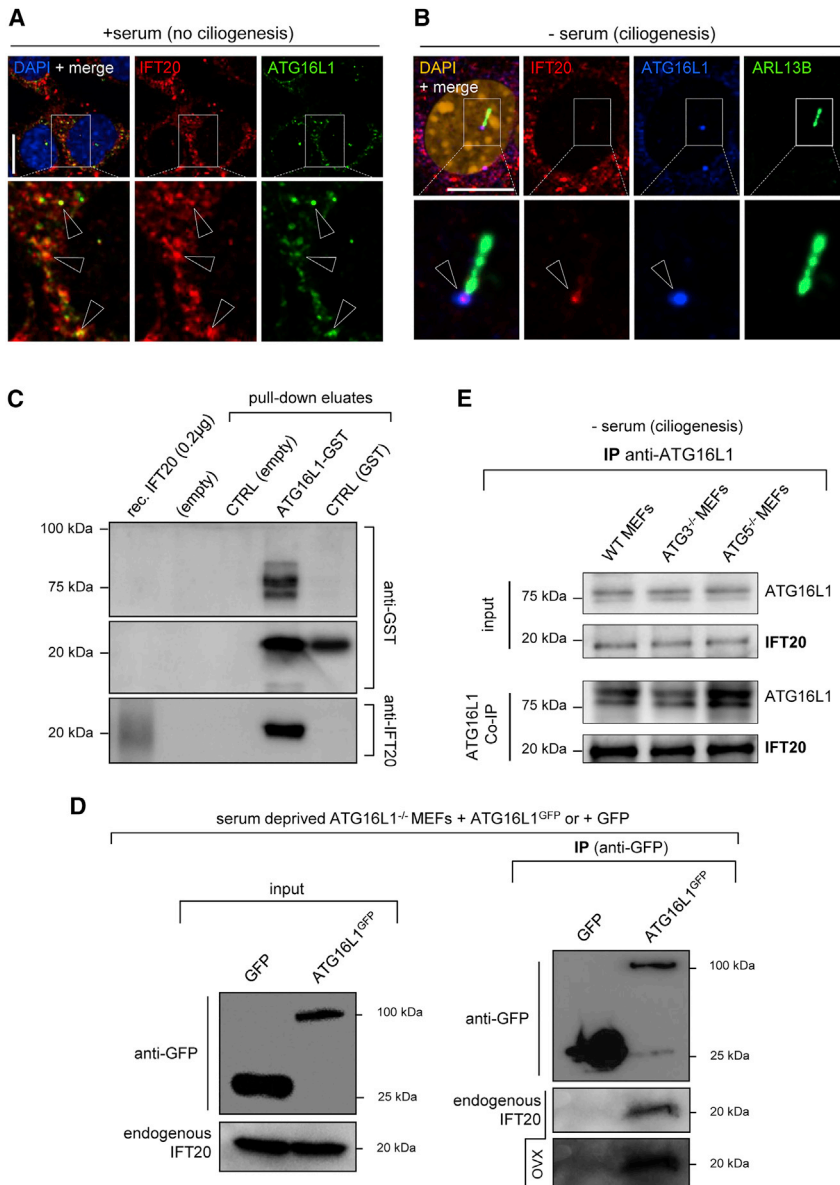


Figure 2. ATG16L1 is present at the PC in ciliated cells and interacts with IFT20

(A and B) Confocal analysis of MEF cells cultured in the presence (A) or 24 h absence (B) of serum and processed for immunofluorescence using DAPI, anti-IFT20, and anti-ATG16L1 antibodies (A) or anti-IFT20, anti-ATG16L1, and anti-ARL13B antibodies (B). Arrowheads show ATG16L1 and IFT20 codistribution in non-ciliated cells (A) and at the base of the PC in (B). Scale bars: 10 μ m.

(C) Pull-down assay to analyze the direct association of ATG16L1 with IFT20. Purified human glutathione S-transferase (GST)-tagged ATG16L1 was conjugated to glutathione-Sepharose beads and, subsequently, incubated with purified IFT20. The elution was analyzed by western blotting using anti-GST and anti-IFT20 antibodies. GST, CTRL (GST); and glutathione-only, CTRL (empty) conditions were used as controls. (D) *Atg16L1*^{GFP} MEFs were transiently transfected with ATG16L1^{GFP} or empty (GFP) expression vectors, cultured in a 24-h absence of serum and processed for co-immunoprecipitation analysis. Total lysates (input) were subjected to immunoprecipitation (IP) with GFP-trap beads. Samples were analyzed by SDS-PAGE and western blotting with anti-GFP and anti-IFT20 antibodies. OVX, overexposed. (E) Wild-type (WT) *Atg3*^{-/-} and *Atg5*^{-/-} MEFs were cultured for 24 h in the absence of serum and processed for co-immunoprecipitation (coIP) analysis. Total lysates (input) were subjected to coIP using anti-ATG16L1 antibody. Samples were analyzed by SDS-PAGE and western blotting with anti-ATG16L1 and anti-IFT20 antibodies.

and IFT20 are part of a complex that does not rely on the autophagy machinery but which handles exocyst subunits in ciliated cells only. These data suggest a role of the ATG16L1/IFT20 complex in Golgi-to-plasma membrane trafficking, a vesicular pathway known to actively participate in ciliogenesis and primary cilium maintenance.

WD40 domain of ATG16L1 and a “YEFI” motif of IFT20 are required for ATG16L1/IFT20 interaction

To further characterize the molecular dialog of ATG16L1 and IFT20, we analyzed the putative binding domains that could afford their interaction. ATG16L1 WD40 repeat domain, which is not required for starvation-associated autophagy (Fletcher et al., 2018), has been reported to be crucial for

protein-protein interactions (Boada-Romero et al., 2013, 2016; Fletcher et al., 2018). We, thus, tested whether this domain could be required for the ATG16L1/IFT20 complex regulation. We compared the ability of wild-type ATG16L1^{GFP} and Δ WD40-ATG16L1^{GFP}, in which the 336–623 aa sequence was removed, to co-immunoprecipitate endogenous IFT20 in *Atg16L1*^{-/-} MEFs (Figure 3A). IFT20 was no longer co-immunoprecipitated in Δ WD40-ATG16L1^{GFP}-rescued cells (Figure 3B), suggesting that the ATG16L1 WD domain is required for IFT20/ATG16L1 interaction.

A putative ATG16L1 binding domain was described in TMEM59, a Golgi-associated protein (Boada-Romero et al., 2013). By sequence analysis, we identified a similar domain in human IFT20 and replaced the four essential amino acids reported to be crucial—Tyr111 (Y), Glu118 (E), Phe124 (F), and Ile129 (I)—with four alanine residues, leading to an IFT20 “YEFI mutant” (Figure 3C). We then tested whether the IFT20-YEFI mutant was still able to interact with ATG16L1. Although in *Ifit20*^{-/-} MEFs transfected with IFT20^{mCherry}, endogenous ATG16L1 co-immunoprecipitated with IFT20^{mCherry}, that was not the case with the YEFI-IFT20^{mCherry} mutant (Figures 3D and 3E), showing that the IFT20 domain was required for ATG16L1 binding.

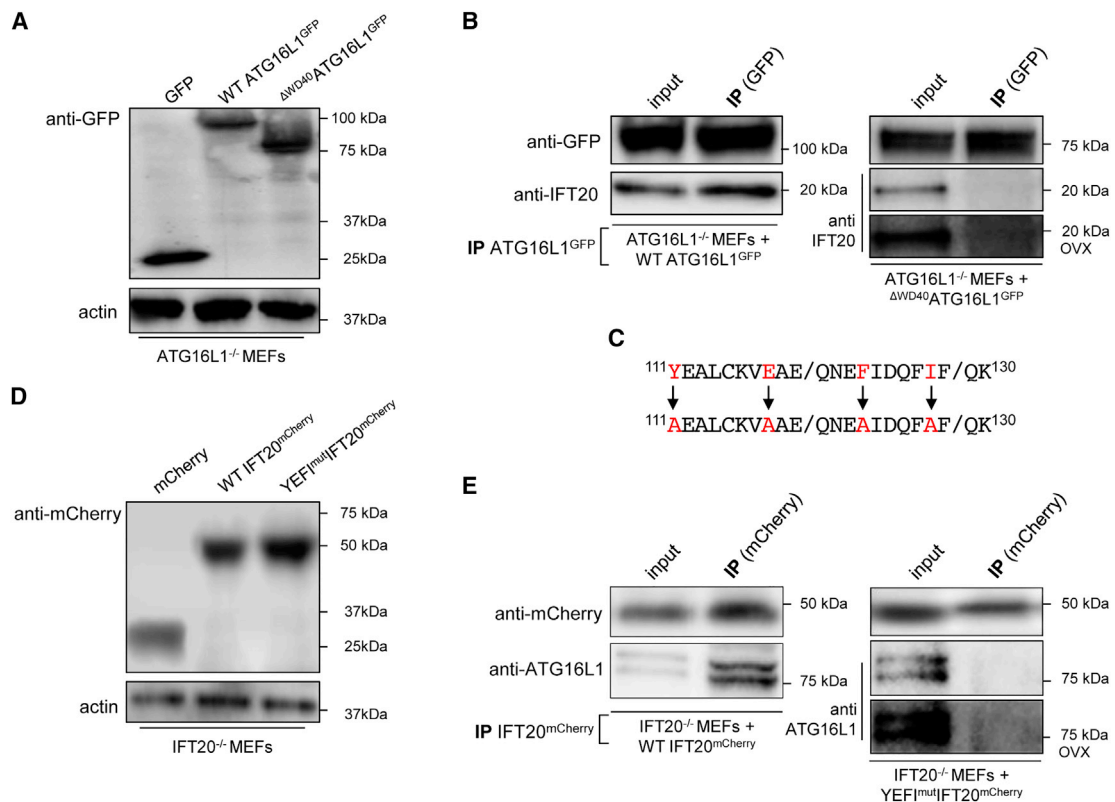


Figure 3. ATG16L1/IFT20 interacting domains

(A and B) *Atg16L1*^{-/-} MEFs were transiently transfected with empty GFP, WT ATG16L1^{GFP}, and Δ WD40-ATG16L1^{GFP} expression vectors, cultured for 24 h in the absence of serum and processed for western blotting analysis (A) and for co-immunoprecipitation, followed by western blotting analysis (B). Total lysates (input) were subjected to IP with GFP-trap beads, and samples were analyzed by SDS-PAGE and western blotting with anti-GFP and anti-IFT20 antibodies.

(C) The 111–130 aa sequence of human IFT20 protein. The key residues mutated (Y, E, F, and I) in the putative ATG16L1 binding sequence are highlighted in red and the YEFI mutant version of IFT20 is shown (bottom sequence, with alanine residues replacing the YEFI residues).

(D and E) *Ift20*^{-/-} MEFs were transiently transfected with empty mCherry, WT IFT20^{mCherry}, and the YEFI mutant of IFT20^{mCherry} expression vectors, cultured for 24 h in the absence of serum and processed for western blotting analysis (D) and for co-immunoprecipitation, followed by western blotting analysis (E). Total lysates (input) were subjected to IP with mCherry/RFP-trap beads, and samples were analyzed by SDS-PAGE and western blotting with anti-mCherry and anti-ATG16L1 antibodies.

We, then, investigated the phenotype associated with the YEFI-IFT20 mutant and asked whether the absence of IFT20 binding to ATG16L1 could have consequences on ciliogenesis. As expected (Figure S2C), ciliogenesis and ATG16L1 recruitment at the PC were inhibited in *Ift20*^{-/-} MEF cells and were rescued upon expression of wild-type IFT20 (Figures 4A, top and middle panels, and 4C). In stark contrast, expression of the ATG16L1 non-binding, IFT20 YEFI mutant could not rescue ciliogenesis (Figures 4A, bottom panel, and 4C). This shows that mutating the ATG16L1-binding motif of IFT20 is sufficient to abrogate IFT20 function in ciliogenesis and confirms the importance of ATG16L1 and IFT20 interaction during ciliogenesis. Accordingly, we show that the IFT20 YEFI mutant no longer colocalizes with ATG16L1 and remains associated with Golgi structures (Figures 4B and 4D).

Absence of ATG16L1 alters ciliogenesis and IFT20 trafficking

To go a step further, we questioned the effect of ATG16L1 knockout (using *Atg16L1*^{-/-} MEFs) on IFT20 subcellular

localization and associated functions at the PC. Unexpectedly, the total absence of ATG16L1 leads to PC overgrowth, as measured by ciliary length ($\pm 8 \mu\text{m}$ in wild-type and $\pm 20 \mu\text{m}$ in *Atg16L1*^{-/-} cells; Figures 5A and 5B), and produced a giant cilium-like structure. This phenotype was rescued by wild-type ATG16L1 expression (Figures 5A and 5B, middle panels). In contrast, we showed a complete loss of ciliogenesis in *Atg16L1*^{-/-} cells transfected with the Δ WD40-ATG16L1 mutant (Figures 5A and 5B), which does not interact with IFT20 (Figure 3). Importantly, we observed that *Atg16L1*^{-/-} cells accumulate IFT20, whereas its levels were strongly reduced in Δ WD40-ATG16L1 transfected *Atg16L1*^{-/-} cells (Figures S6A–S6C). This situation is reminiscent of what is observed in the presence of serum, a condition that represses ciliogenesis (Figures 1D and 1F). Interestingly, the level of IFT20 was shown to be negatively regulated by autophagy in the presence of serum (Pampliega et al., 2013). On the other hand, the WD domain of ATG16L1 is dispensable for canonical autophagy during starvation (Fletcher et al., 2018). Indeed,

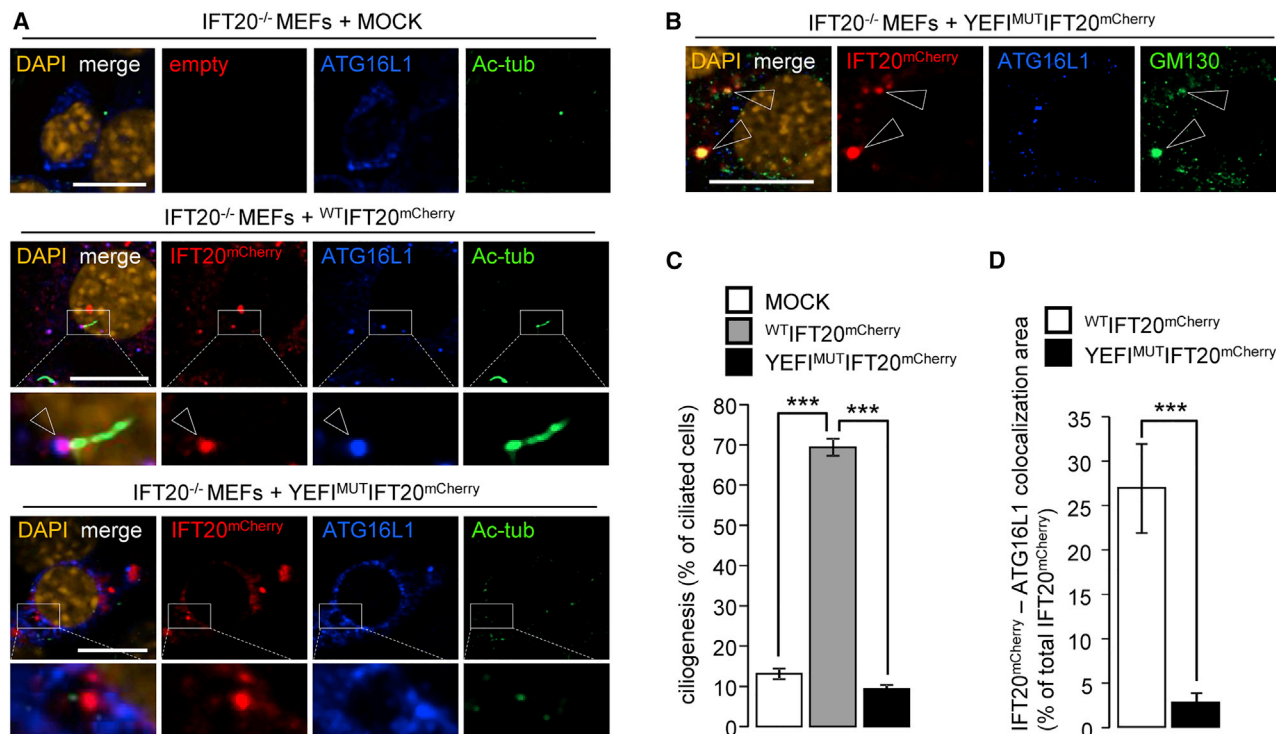


Figure 4. Loss of ATG16L1 binding motif in IFT20 leads to IFT20 Golgi retention and ciliogenesis defect

(A) *Ift20*^{-/-} MEFs were transiently transfected with WT IFT20^{mCherry} (middle panel) and YEF1 mutant of IFT20^{mCherry} (bottom panel) expression vectors or not (mock, top panel), cultured for 24 h in the absence of serum and processed for immunofluorescence analysis using anti-acetylated tubulin (Ac-tub) and anti-ATG16L1. Arrowheads show WT-IFT20^{mCherry} colocalization with endogenous ATG16L1 at the base of the PC (A, middle panel). Scale bar: 10 μ m.

(B) *Ift20*^{-/-} MEFs were transiently transfected with the YEF1 mutant of IFT20^{mCherry} (bottom panel) expression vectors cultured for 24 h in the absence of serum and processed for immunofluorescence analysis using anti-GM130 and anti-ATG16L1. Arrowheads show YEF1 mutant of IFT20^{mCherry} colocalization with GM130 and the absence of colocalization with ATG16L1. Scale bar: 8 μ m.

(C) Bar diagram showing the quantification of ciliogenesis (as expressed by the percentage of ciliated cells) in WT IFT20^{mCherry} and YEF1 mutant of IFT20^{mCherry} conditions.

(D) Bar diagram showing the quantification of endogenous ATG16L1/IFT20^{mCherry} colocalization area (as expressed by the percentage of total IFT20^{mCherry} signal) in WT IFT20^{mCherry} and YEF1 mutant of IFT20^{mCherry} conditions.

In (C) and (D), values denote means \pm SEM. ****p* < 0.001 using the Student's *t* test (*n* = 75 cells from three independent experiments).

expression of Δ WD40-ATG16L1 in *Atg16L1*^{-/-} cells promotes a partial rescue of the autophagic capacity, as observed by LC3 western blot analysis (Figures S6D and S6E) and LC3 immunofluorescence (Figures S6F and S6G) in starvation conditions. These results suggest that the presence of Δ WD40-ATG16L1, which does not interact with IFT20, is sufficient to support autophagy, which, in turns, leads to IFT20 degradation and, consequently, inhibits ciliogenesis (Figures 5A and 5B); however, in *Atg16L1*^{-/-} cells (in which canonical autophagy is inhibited), longer ciliary structure is observed.

These intriguing data suggested that ATG16L1 could be required, independent of its autophagic activity, for the regulation of ciliogenesis and/or PC morphology and dynamic turnover. In line with that hypothesis, we observed that the IFT20 subcellular pattern was different in serum-deprived *Atg16L1*^{-/-} MEFs compared with that of wild-type cells, with a significant increase of vesicular IFT20⁺ structures (Figures S6A and S7A), which could account for a defect in vesicular trafficking of the protein because IFT20 also massively colocalized with the Golgi marker GM130 (Figure S7B), as classically observed in non-ciliated cells

(Figure 1). Importantly, IFT20 was absent from the axoneme of giant ciliary structures that were observed in *Atg16L1*^{-/-} cells (Figure 5C). In line with that observation, we show that the primary components of the PC axoneme, such as KIF3A or IFT88 (Nachury et al., 2010; Wheway et al., 2018), were no longer present in the axoneme of giant ciliary-like structures of ATG16L1 knockout cells, but are colocalized at the basal body stained with anti- γ -tubulin antibodies (Figure S8).

To investigate the functionality of the ciliary structure in *Atg16L1*^{-/-} MEFs, we analyzed the Hedgehog (Hh) signaling pathway because it is dependent on the PC and on intact IFT trafficking (Rohatgi et al., 2007; Liem et al., 2012). We showed that Gli1, an effector of the Hh pathway associated with PC, stability was affected in serum-deprived *Atg16L1*^{-/-} MEFs (Figures 5D and 5E). Activation of the Hh signaling pathway can be as well monitored by transcriptional activation and local recruitment of its receptor Smoothened (SMO) at the axoneme of the PC (Chávez et al., 2015). Treatment of serum-deprived control MEFs with the SMO agonist purmorphamine leads, as expected, to an increase in SMO mRNA level in wild-type MEFs (Figure 5F).

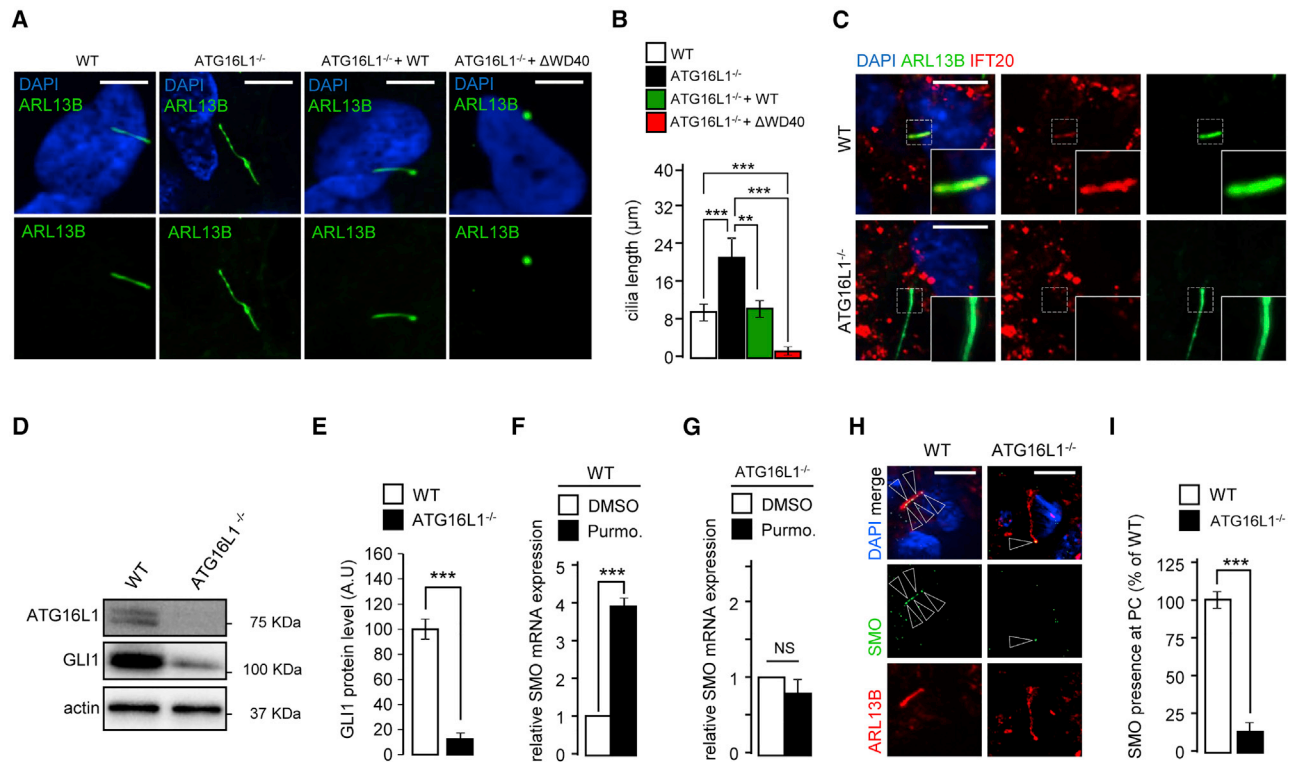


Figure 5. ATG16L1 knockout promotes aberrant ciliogenesis and alters ciliary signaling

(A) WT or *Atg16L1*^{-/-} MEFs transiently transfected (or not) with WT ATG16L1^{GFP} or ΔWD40-ATG16L1^{GFP} expression vectors were cultured for 24 h in the absence of serum and processed for immunofluorescence analysis using DAPI and anti-ARL13B antibody. Scale bar: 10 μm.

(B) Bar graph showing the quantification of the PC axoneme length measured via ARL13B staining, as shown in (A), in WT MEFs or in *Atg16L1*^{-/-} MEFs transfected with WT ATG16L1^{GFP} or ΔWD40-ATG16L1^{GFP} (ΔWD40). Values denote means ± SEM. **p < 0.01, ***p < 0.001 using the Student's t test (n = 60 cells from three independent experiments).

(C) WT or *Atg16L1*^{-/-} MEFs were cultured for 24 h in the absence of serum and processed for immunofluorescence analysis using DAPI and anti-ARL13B and anti-IFT20 antibodies. Scale bar: 10 μm.

(D) WT or *Atg16L1*^{-/-} MEFs were cultured for 24 h in the absence of serum and processed for western blotting analysis using anti-ATG16L1, anti-GLI1, and anti-actin antibodies.

(E) Bar diagram showing the quantification of relative GLI1 protein levels shown in (D) in WT or *Atg16L1*^{-/-} MEFs. Values denote means ± SEM. ***p < 0.001 using the Student's t test (n = 3 independent experiments).

(F and G) WT (F) or *Atg16L1*^{-/-} (G) MEFs were cultured for 24 h in the absence of serum, stimulated (or not, DMSO) with 5 μM of Smoothed (SMO) agonist purmorphamine and processed for SMO mRNA quantification. Values denote means ± SD. ***p < 0.001 using the Student's t test (n = 5 independent experiments). NS, not significant.

(H) WT or *Atg16L1*^{-/-} MEFs were cultured for 24 h in the absence of serum and processed for immunofluorescence analysis using DAPI, anti-ARL13B, and anti-SMO antibodies. Scale bar: 10 μm.

(I) Bar diagram showing the quantification of the SMO presence at the PC, as a percentage of the WT condition, as illustrated in (H) in WT or *Atg16L1*^{-/-} MEFs. Values denote means ± SEM. ***p < 0.001 using the Student's t test (n = 50 cells from three independent experiments).

However, purmorphamine failed to induce a similar increase in *Atg16L1*^{-/-} cells (Figure 5G), suggesting that the Hh signaling response is deficient in the absence of ATG16L1, even in the presence of the giant cilium-like-associated structures that we observed in *Atg16L1*^{-/-} cells. Finally, we showed that although SMO was indeed recruited massively to the PC in wild-type cells, SMO was almost absent from the giant ciliary structure produced in *Atg16L1*^{-/-} MEFs (Figures 5H and 5I). Overall, the data demonstrate that PC-associated Hh signaling was not active in the absence of ATG16L1. This was further supported by the abnormal subcellular distribution of the G-receptor GPR161, an Hh pathway repressor during ciliogenesis (Mukhopadhyay et al., 2013). In wild-type, ciliated cells, GPR161 is

restricted to the base of the PC, whereas in *Atg16L1*^{-/-} cells, it accumulates in the axoneme of the giant ciliary structures (Figure S9). Thus, the giant, but nonfunctional, cilium-like protrusion observed in *Atg16L1*^{-/-} cells (Figure 5) directly questions the identity of ciliary components and the membrane in this specific situation.

One of the key features of the regulation of ciliary structure and function is the tight phosphoinositides equilibrium established at the interface of axonemal and plasma membranes at the base of the PC (Shewan et al., 2011; Fry et al., 2014; Nakatsu, 2015; Schink et al., 2016; Conduit and Vanhaesebroeck, 2020). Like for some Golgian subdomains, the PC is enriched in PI4P at the axonemal membrane but is depleted in PI4,5P2, except at

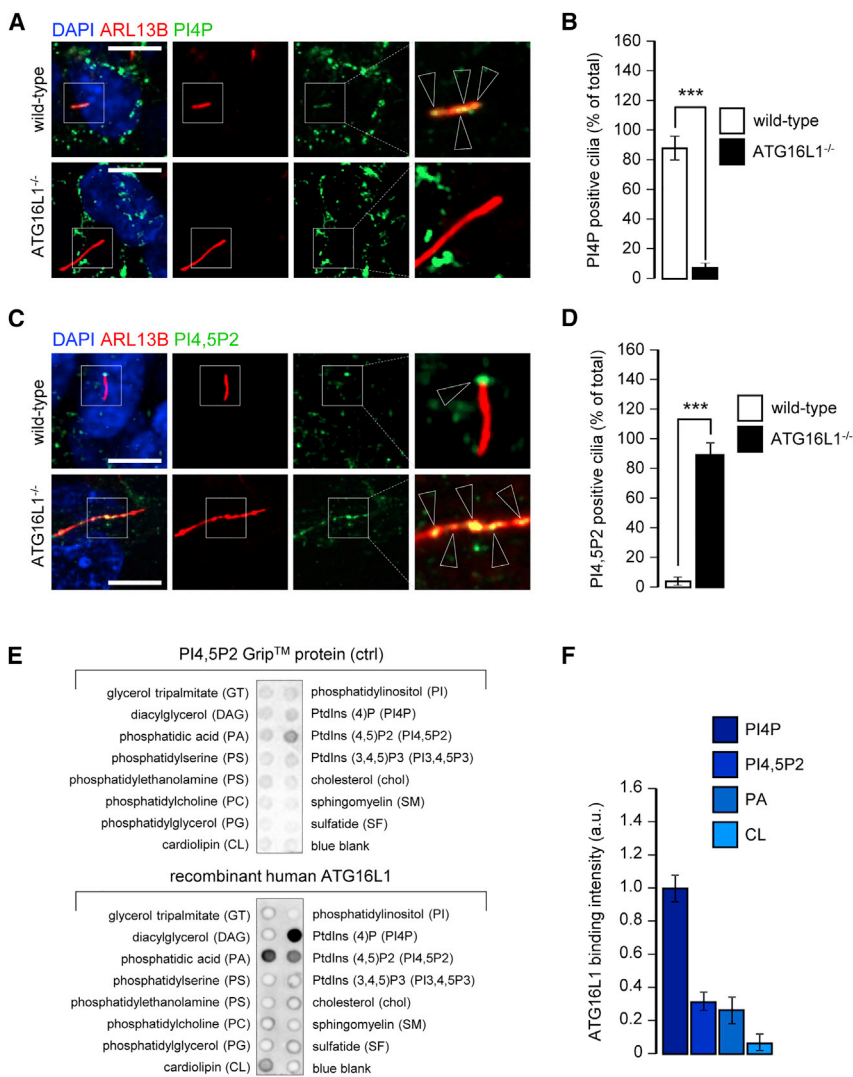


Figure 6. PC-associated PI4P and PI4,5P2 turnover is altered in the absence of ATG16L1

(A) WT or *Atg16L1*^{-/-} MEFs were cultured for 24 h in the absence of serum and processed for immunofluorescence analysis using DAPI, anti-ARL13B, and anti-PI4P antibodies. Arrowheads denote the co-distribution of PI4P⁺ puncta with the PC, only in the WT condition. Scale bars: 10 μ m.

(B) Bar diagram showing the quantification of PI4P⁺ axonemes (expressed as the percentage of total cilia), as illustrated in (A), in WT, or *Atg16L1*^{-/-} MEFs. Values denote means \pm SEM. ***p < 0.001 using the Student's t test (n = 80 cells from four independent experiments).

(C) WT or *Atg16L1*^{-/-} MEFs were cultured for 24 h in the absence of serum and processed for immunofluorescence analysis using DAPI, anti-ARL13B, and anti-PI4,5P2 antibodies. Arrowheads denote localization of PI4,5P2 only at the base of the PC (in the WT cells) or in the axoneme (in *Atg16L1*^{-/-} MEFs). Scale bars: 10 μ m.

(D) Bar diagram showing the quantification of PI4,5P2⁺ axonemes (expressed as the percentage of total cilia), as illustrated in (C), in WT, or *Atg16L1*^{-/-} MEFs. Values denote means \pm SEM. ***p < 0.001 using Student's t test (n = 80 cells from four independent experiments).

(E) Lipid strip probed with Gip-protein-positive control for PI4,5P2 (top panel) and with human recombinant ATG16L1, followed by secondary antibody conjugated with peroxidase for visualization. (F) Bar diagram showing the quantification of recombinant ATG16L1 binding on the lipid strip (E) with positive values: PI4P, PI4,5P2, phosphatidic acid (PA), and cardiolipin (CL) (from three independent experiments).

the base of the PC membrane (Nakatsu, 2015; Conduit and Vanhaesebroeck, 2020). We, thus, tested the PI4P and PI4,5P2 relative distribution at the PC of *Atg16L1*-depleted cells. We observed that the giant ciliary-like protrusions observed in *Atg16L1*^{-/-} cells were devoid of PI4P (Figures 6A and 6B) whereas their axonemes showed an aberrant accumulation of PI4,5P2 (Figures 6C and 6D).

Moreover, we show that recombinant, purified, human ATG16L1 was able to bind to purified PI4P and PI4,5P2 from *in vitro* lipid-strip experiments (Figures 6E and 6F), suggesting a direct association of membrane-bound ATG16L1 on PI4,5P2 and PI4P⁺ vesicles *in vivo*.

The phosphoinositide turnover at the PC depends on ATG16L1/INPP5E dialog

The altered PI4P/PI4,5P2 equilibrium observed at the PC of *Atg16L1* knocked out cells might be related to INPP5E, a crucial lipid phosphatase implicated in cilia membrane turnover

PI4,5P2 decrease in the target membrane. Upon serum deprivation, a pool of INPP5E localizes at the PC in wild-type cells (Figures 7C, top panels, and 7D). In *Atg16L1*^{-/-} MEFs, although the total cellular amount of INPP5E was not affected (Figures 7A and 7B), the giant ciliary-like structures were devoid of INPP5E (Figures 7C, bottom panels, and 7D), suggesting that INPP5E trafficking to the PC was affected in those cells.

We, thus, wondered whether INPP5E could be a partner of ATG16L1 and IFT20 in vesicular trafficking leading from the Golgi to the PC. In *Atg16L1*^{-/-} cells expressing ATG16L1^{GFP}, INPP5E co-immunoprecipitated with ATG16L1 (Figure 7E), whereas INPP5E was not co-immunoprecipitated from *Atg16L1*^{-/-} MEFs expressing Δ WD40 ATG16L1 (Figure 7F). This result strongly suggests that the interaction between IFT20 and ATG16L1 is required for INPP5E to be a component of the ATG16L1 complex.

Altogether, our results suggest that ATG16L1 interacts with INPP5E and that the ATG16L1/INPP5E/IFT20 complex is

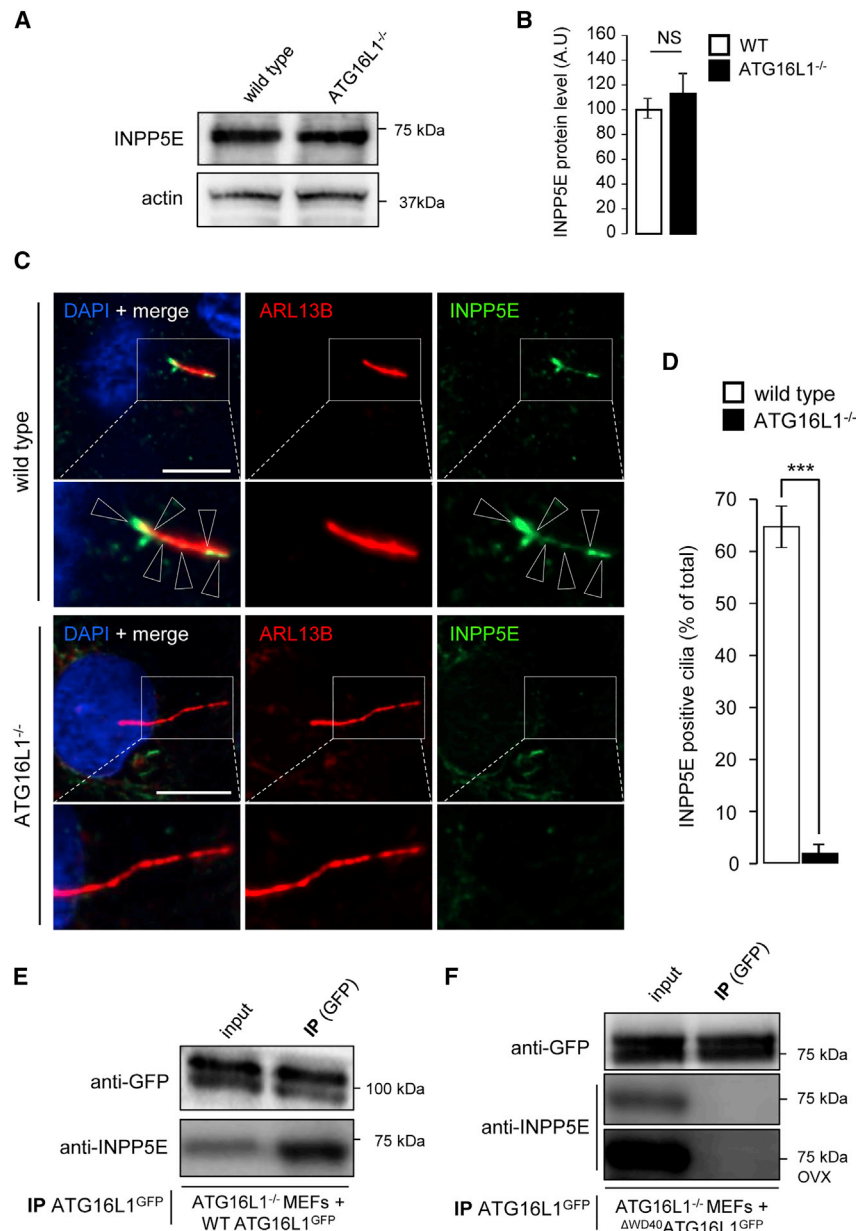


Figure 7. INPP5E phosphatase is a key partner of ATG16L1 during ciliogenesis

(A) WT or *Atg16L1*^{-/-} MEFs were cultured for 24 h in the absence of serum and processed for western blotting analysis using anti-INPP5E and anti-actin antibodies.

(B) Bar diagram showing the quantification of relative INPP5E protein levels shown in (A) in WT or *ATG16L1*^{-/-} MEFs. Values denote means ± SEM. NS, not significant (n = 3 independent experiments).

(C) WT or *ATG16L1*^{-/-} MEFs were cultured for 24 h in the absence of serum and processed for immunofluorescence analysis using DAPI, anti-ARL13B, and anti-INPP5E antibodies. Arrowheads denote codistribution of INPP5E⁺ puncta with the PC (only in the WT condition). Scale bar: 8 μm.

(D) Bar diagram showing the quantification of INPP5E⁺ axonemes (expressed as the percentage of total cilia), as illustrated in (C), in WT or *Atg16L1*^{-/-} MEFs. Values denote means ± SEM. ***p < 0.001 using the Student's t test (n = 75 cells from three independent experiments).

(E and F) *ATG16L1*^{-/-} MEFs were transiently transfected with WT *ATG16L1*^{GFP} (E) or ΔWD40-*ATG16L1*^{GFP} (F) expression vectors, cultured for 24 h in the absence of serum, and processed for co-immunoprecipitation analysis. Total lysates (input) were subjected to IP with GFP-trap beads, and samples were analyzed by SDS-PAGE and western blotting with anti-GFP and anti-INPP5E antibodies.

conditions (Pampliega et al., 2013). Although the CCD domain of *ATG16L1* is essential for its autophagy-related functions (such as *ATG5* interaction) (Fujita et al., 2008), its WD40 domain, a seven repetition of the WD motif important in protein-protein interactions (Xu and Min, 2011), is not essential for classical autophagy (Fletcher et al., 2018). We now report that the WD40 domain of *ATG16L1* is required for interactions with the ciliogenesis-related protein IFT20. Reciprocally, based on data highlighted in *TMEM59B* and *ATG16L1* interaction (Boada-Romero et al., 2013), we identified an *ATG16L1*-binding domain in the C-terminal part of IFT20 (with four

essential amino acids, which constitute what we reported as a YEFI motif [Tyr-Glu-Phe-Ile]. Mutation of the YEFI motif is sufficient to block IFT20 in the Golgi apparatus and alter ciliogenesis. Our results indicate that the WD40-*ATG16L1* and YEFI-IFT20 domains are required for the proper intracellular targeting of the *ATG16L1*-IFT20 complex to the PC in response to serum deprivation, potentially with the exocyst protein *SEC8*. However, amino acid modifications in, or within proximity of, WD40 could balance the interaction of *ATG16L1* with other partners (Boada-Romero et al., 2016).

DISCUSSION

The interconnection between the PC and the autophagic machinery discovered less than 10 years ago (Pampliega et al., 2013; Tang et al., 2013) raised several questions about the ins and outs of such functional crosstalk and its direct implication(s) on both autophagy and ciliogenesis. Here, we confirm the interaction between IFT20 and *ATG16L1* in both ciliated and non-ciliated

required to ensure membrane local depletion of PI4,5P2 and PI4P synthesis at dedicated membranes, presumably, on Golgi-derived vesicles (suggested by the presence of *Sec8* during ciliogenesis) en route to the PC.

In the absence of *ATG16L1* and upon serum deprivation, a giant cilium-like protrusion is formed from the plasma membrane. Long, cilia-like structures have also been observed in

the absence of other ATG proteins (Pampliega et al., 2013). Here, we show that these cilia-like structures display some markers of the PC, such as γ -tubulin and ARL13B, and lack other ciliary markers, such as IFT88 and KIF3a. We show that Hh signaling is impaired in the cilia-like structures, implying that they are, at least partly, dysfunctional. However, the ciliary phenotype observed in ATG16L1-depleted cells is not due to a canonical autophagy defect because the ATG16L1 and IFT20 interaction is independent of ATG5 and ATG3, both key components of the canonical autophagic machinery. In addition, Beclin1 and its kinase partner VPS34 are likewise not part of the IFT20-ATG16L1 complex. Finally, and importantly, we show that the Δ WD40 autophagy-competent version of ATG16L1, which does not interact with IFT20 and alters its trafficking, is not able to rescue ciliogenesis in ATG16L1-depleted cells.

Phosphoinositides are key regulators of cellular organelles identity (Di Paolo and De Camilli, 2006). The PC membrane is depleted of PI4,5P2 and enriched in PI4P (Chávez et al., 2015; Nakatsu, 2015; Phua et al., 2018). Here, we report that purified ATG16L1 interacts with PI4P and, to a lesser extent, with PI(4.5)P2, confirming the recently reported ability of ATG16L1 to bind PI3P, PI4P, and PI4,5P2 (Dudley et al., 2019). ATG16L1 direct lipid binding was proposed to require the 28–44 aa region of the protein (Lystad et al., 2019); however, its coiled-coil domain (120–206 aa) was also described as being required for PI3P binding (Dudley et al., 2019). ATG16L1 dissection, to identify its PI4P-binding domain, is beyond the scope of this study; however, by merging all recent data, including those described here, we can hypothesize that different pools of ATG16L1 coexist at different trafficking stations, probably in different protein complexes, for, supposedly, different stress-related processes.

Our study shows that the absence of ATG16L1 alters the distribution of ciliary phosphoinositides. PI4P is depleted from the giant cilium-like “axoneme,” which is, in turn, enriched in PI4,5P2. This explains the impaired SMO and Hh signaling observed in *Atg16L1*-null cells. These results suggest that PC-phosphoinositide equilibrium depends, at least partially, on ATG16L1.

We show that INPP5E, which is a cilia and Golgi-localized inositol 5-phosphatase associated with the Joubert syndrome (Braun and Hildebrandt, 2017), is part of the ATG16L1-IFT20 complex. INPP5E is responsible for PI4P production at the PC (Bielas et al., 2009; Xu et al., 2016, 2017). Our results suggest that depletion of ATG16L1 inhibits INPP5E trafficking to the PC membrane. It is, thus, tempting to hypothesize that the PI4,5P2 axonemal accumulation occurring in the giant cilium-like protrusion of *Atg16L1* knockout cells is due to a defect in targeting of IFT20/INPP5E vesicles to their proper subcellular localization, i.e., the site of PC biogenesis.

Our data highlight the importance of ATG16L1 in the stress-associated trafficking of INPP5E, which is directly connected to PC membrane identity regulation and is independent of ATG16L1 functions in canonical autophagy. Further experiments must clarify the probable other differences in the membrane composition and/or dynamics between wild-type and *Atg16L1* knockout cells, in response to serum deprivation.

Altogether, our results suggest a role for ATG16L1 in lipid-dynamic, ciliary-protein trafficking; in which, the protein directly participates in ciliogenesis regulation and identity in response to sensing stress.

STAR★METHODS

Detailed methods are provided in the online version of this paper and include the following:

- KEY RESOURCES TABLE
- RESOURCE AVAILABILITY
 - Lead contact
 - Materials availability
 - Data and code availability
- EXPERIMENTAL MODEL AND SUBJECT DETAILS
 - Cell lines
 - Cell transfection
- METHOD DETAILS
 - Cell treatments
 - Protein extraction and western blotting analysis
 - *In vitro* pull-down assay
 - Immunofluorescence microscopy and imaging
 - Real time quantitative PCR
 - GFP-trap and RFP-trap assays
 - Lipid overlay assay
- QUANTIFICATION AND STATISTICAL ANALYSIS

SUPPLEMENTAL INFORMATION

Supplemental information can be found online at <https://doi.org/10.1016/j.celrep.2021.109045>.

ACKNOWLEDGMENTS

We warmly thank S. Tooze, A.M. Cuervo, G.J. Pazour, M. Komatsu, and N. Mizushima for kindly sharing cells and reagents with us. We thank our colleagues at INEM/INSERM U1151 for fruitful discussions and support. We thank E. Boëdec, T. Galli, and V. Goffin for sharing advice on *in vitro* pull-down experiments. We thank Z. Chamoun for critical reading of the manuscript. This work was supported by institutional funding from INSERM, CNRS, Université de Paris, and grants from the EU (“Innovative training network on autophagy drive” 765912) and Agence Nationale de la Recherche (ANR; ANR-17-CE140030-02, ANR-17-CE13-0015-003, and ANR-18-CE14-0026-02).

AUTHOR CONTRIBUTIONS

A.B. performed most of the biological and biochemical experiments and analyses; F.R. and N.D. contributed to biochemical analyses and contributed to the paper editing; P.C. co-supervised the project and contributed to the paper writing and editing; E.M. contributed to imaging and biochemical experiments, analyzed and quantified the cell biological assays and fluorescence data, supervised the project, and wrote the paper.

DECLARATION OF INTERESTS

The authors declare no competing interests.

Received: December 9, 2019

Revised: February 22, 2021

Accepted: April 7, 2021

Published: April 27, 2021

REFERENCES

- Bento, C.F., Renna, M., Ghislat, G., Puri, C., Ashkenazi, A., Vicinanza, M., Menzies, F.M., and Rubinsztein, D.C. (2016). Mammalian autophagy: how does it work? *Annu. Rev. Biochem.* **85**, 685–713.
- Bielas, S.L., Silhavy, J.L., Brancati, F., Kisseleva, M.V., Al-Gazali, L., Sztrihai, L., Bayoumi, R.A., Zaki, M.S., Abdel-Aleem, A., Rosti, R.O., et al. (2009). Mutations in INPP5E, encoding inositol polyphosphate-5-phosphatase E, link phosphatidylinositol signaling to the ciliopathies. *Nat. Genet.* **41**, 1032–1036.
- Boada-Romero, E., Letek, M., Fleischer, A., Pallauf, K., Ramón-Barros, C., and Pimentel-Muñoz, F.X. (2013). TMEM59 defines a novel ATG16L1-binding motif that promotes local activation of LC3. *EMBO J.* **32**, 566–582.
- Boada-Romero, E., Serramito-Gómez, I., Sacristán, M.P., Boone, D.L., Xavier, R.J., and Pimentel-Muñoz, F.X. (2016). The T300A Crohn's disease risk polymorphism impairs function of the WD40 domain of ATG16L1. *Nat. Commun.* **7**, 11821.
- Boukhalfa, A., Miceli, C., Ávalos, Y., Morel, E., and Dupont, N. (2019). Interplay between primary cilia, ubiquitin-proteasome system and autophagy. *Biochimie* **166**, 286–292.
- Boukhalfa, A., Nascimbeni, A.C., Ramel, D., Dupont, N., Hirsch, E., Gayral, S., Laffargue, M., Codogno, P., and Morel, E. (2020). PI3KC2 α -dependent and VPS34-independent generation of PI3P controls primary cilium-mediated autophagy in response to shear stress. *Nat. Commun.* **11**, 294.
- Boya, P., Reggiori, F., and Codogno, P. (2013). Emerging regulation and functions of autophagy. *Nat. Cell Biol.* **15**, 713–720.
- Braun, D.A., and Hildebrandt, F. (2017). Ciliopathies. *Cold Spring Harb. Perspect. Biol.* **9**, a028191.
- Cao, M., and Zhong, Q. (2016). Cilia in autophagy and cancer. *Cilia* **5**, 4.
- Chávez, M., Ena, S., Van Sande, J., de Kerchove d'Exaerde, A., Schurmans, S., and Schiffmann, S.N. (2015). Modulation of ciliary phosphoinositide content regulates trafficking and sonic hedgehog signaling output. *Dev. Cell* **34**, 338–350.
- Cloonan, S.M., Lam, H.C., Ryter, S.W., and Choi, A.M. (2014). “Ciliophagy”: the consumption of cilia components by autophagy. *Autophagy* **10**, 532–534.
- Conduit, S.E., and Vanhaesebroeck, B. (2020). Phosphoinositide lipids in primary cilia biology. *Biochem. J.* **477**, 3541–3565.
- De La Iglesia, F.A., and Porta, E.A. (1967). Ciliated biliary epithelial cells in the livers of non-human primates. *Experientia* **23**, 49–51.
- Di Paolo, G., and De Camilli, P. (2006). Phosphoinositides in cell regulation and membrane dynamics. *Nature* **443**, 651–657.
- Dudley, L.J., Cabodevilla, A.G., Makar, A.N., Sztacho, M., Michelberger, T., Marsh, J.A., Houston, D.R., Martens, S., Jiang, X., and Gammoh, N. (2019). Intrinsic lipid binding activity of ATG16L1 supports efficient membrane anchoring and autophagy. *EMBO J.* **38**, e100554.
- Fletcher, K., Ulferts, R., Jacquin, E., Veith, T., Gammoh, N., Arasteh, J.M., Mayer, U., Carding, S.R., Wileman, T., Beale, R., and Florey, O. (2018). The WD40 domain of ATG16L1 is required for its non-canonical role in lipidation of LC3 at single membranes. *EMBO J.* **37**, e97840.
- Fogelgren, B., Lin, S.Y., Zuo, X., Jaffe, K.M., Park, K.M., Reichert, R.J., Bell, P.D., Burdine, R.D., and Lipschutz, J.H. (2011). The exocyst protein Sec10 interacts with Polycystin-2 and knockdown causes PKD-phenotypes. *PLoS Genet.* **7**, e1001361.
- Follit, J.A., Tuft, R.A., Fogarty, K.E., and Pazour, G.J. (2006). The intraflagellar transport protein IFT20 is associated with the Golgi complex and is required for cilia assembly. *Mol. Biol. Cell* **17**, 3781–3792.
- Follit, J.A., San Agustín, J.T., Xu, F., Jonassen, J.A., Samtani, R., Lo, C.W., and Pazour, G.J. (2008). The Golgin GMAP210/TRIP11 anchors IFT20 to the Golgi complex. *PLoS Genet.* **4**, e1000315.
- Fry, A.M., Leaper, M.J., and Bayliss, R. (2014). The primary cilium: guardian of organ development and homeostasis. *Organogenesis* **10**, 62–68.
- Fujita, N., Itoh, T., Omori, H., Fukuda, M., Noda, T., and Yoshimori, T. (2008). The Atg16L complex specifies the site of LC3 lipidation for membrane biogenesis in autophagy. *Mol. Biol. Cell* **19**, 2092–2100.
- García-Gonzalo, F.R., Phua, S.C., Roberson, E.C., García, G., 3rd, Abedin, M., Schurmans, S., Inoue, T., and Reiter, J.F. (2015). Phosphoinositides regulate ciliary protein trafficking to modulate hedgehog signaling. *Dev. Cell* **34**, 400–409.
- Goetz, S.C., and Anderson, K.V. (2010). The primary cilium: a signalling centre during vertebrate development. *Nat. Rev. Genet.* **11**, 331–344.
- Hardee, I., Soldatos, A., Davids, M., Vilboux, T., Toro, C., David, K.L., Ferreira, C.R., Nehrebecky, M., Snow, J., Thurm, A., et al. (2017). Defective ciliogenesis in INPP5E-related Joubert syndrome. *Am. J. Med. Genet. A.* **173**, 3231–3237.
- He, M., Agbu, S., and Anderson, K.V. (2017). Microtubule motors drive hedgehog signaling in primary cilia. *Trends Cell Biol.* **27**, 110–125.
- Izawa, I., Goto, H., Kasahara, K., and Inagaki, M. (2015). Current topics of functional links between primary cilia and cell cycle. *Cilia* **4**, 12.
- Jacoby, M., Cox, J.J., Gayral, S., Hampshire, D.J., Ayub, M., Blockmans, M., Pernot, E., Kisseleva, M.V., Compère, P., Schiffmann, S.N., et al. (2009). INPP5E mutations cause primary cilium signaling defects, ciliary instability and ciliopathies in human and mouse. *Nat. Genet.* **41**, 1027–1031.
- Joffre, C., Dupont, N., Hoa, L., Gomez, V., Pardo, R., Gonçalves-Pimentel, C., Achard, P., Bettoun, A., Meunier, B., Bauvy, C., et al. (2015). The pro-apoptotic STK38 kinase is a new Beclin1 partner positively regulating autophagy. *Curr. Biol.* **25**, 2479–2492.
- Lam, H.C., Cloonan, S.M., Bhashyam, A.R., Haspel, J.A., Singh, A., Sathirapongsasuti, J.F., Cervo, M., Yao, H., Chung, A.L., Mizumura, K., et al. (2013). Histone deacetylase 6-mediated selective autophagy regulates COPD-associated cilia dysfunction. *J. Clin. Invest.* **123**, 5212–5230.
- Levine, B., and Kroemer, G. (2019). Biological functions of autophagy genes: a disease perspective. *Cell* **176**, 11–42.
- Li, J., Chen, Z., Stang, M.T., and Gao, W. (2017). Transiently expressed ATG16L1 inhibits autophagosome biogenesis and aberrantly targets RAB11-positive recycling endosomes. *Autophagy* **13**, 345–358.
- Liem, K.F., Jr., Ashe, A., He, M., Satir, P., Moran, J., Beier, D., Wicking, C., and Anderson, K.V. (2012). The IFT-A complex regulates Shh signaling through cilia structure and membrane protein trafficking. *J. Cell Biol.* **197**, 789–800.
- Luo, N., Lu, J., and Sun, Y. (2012). Evidence of a role of inositol polyphosphate 5-phosphatase INPP5E in cilia formation in zebrafish. *Vision Res.* **75**, 98–107.
- Lystad, A.H., Carlsson, S.R., de la Ballina, L.R., Kauffman, K.J., Nag, S., Yoshimori, T., Melia, T.J., and Simonsen, A. (2019). Distinct functions of ATG16L1 isoforms in membrane binding and LC3B lipidation in autophagy-related processes. *Nat. Cell Biol.* **21**, 372–383.
- Malicki, J.J., and Johnson, C.A. (2017). The cilium: cellular antenna and central processing unit. *Trends Cell Biol.* **27**, 126–140.
- Miceli, C., Roccio, F., Penalva-Mousset, L., Burtin, M., Leroy, C., Nemazany, I., Kuperwasser, N., Pontoglio, M., Friedlander, G., Morel, E., et al. (2020). The primary cilium and lipophagy translate mechanical forces to direct metabolic adaptation of kidney epithelial cells. *Nat. Cell Biol.* **22**, 1091–1102.
- Monis, W.J., Faundez, V., and Pazour, G.J. (2017). BLOC-1 is required for selective membrane protein trafficking from endosomes to primary cilia. *J. Cell Biol.* **216**, 2131–2150.
- Morleo, M., and Franco, B. (2019). The autophagy-cilia axis: an intricate relationship. *Cells* **8**, 905.
- Mukhopadhyay, S., Wen, X., Ratti, N., Loktev, A., Rangell, L., Scales, S.J., and Jackson, P.K. (2013). The ciliary G-protein-coupled receptor Gpr161 negatively regulates the Sonic hedgehog pathway via cAMP signaling. *Cell* **152**, 210–223.
- Nachury, M.V., and Mick, D.U. (2019). Establishing and regulating the composition of cilia for signal transduction. *Nat. Rev. Mol. Cell Biol.* **20**, 389–405.
- Nachury, M.V., Seeley, E.S., and Jin, H. (2010). Trafficking to the ciliary membrane: how to get across the periciliary diffusion barrier? *Annu. Rev. Cell Dev. Biol.* **26**, 59–87.

- Nakatsu, F. (2015). A phosphoinositide code for primary cilia. *Dev. Cell* *34*, 379–380.
- Nascimbeni, A.C., Codogno, P., and Morel, E. (2017). Phosphatidylinositol-3-phosphate in the regulation of autophagy membrane dynamics. *FEBS J.* *284*, 1267–1278.
- Nishida-Fukuda, H. (2019). The exocyst: dynamic machine or static tethering complex? *BioEssays* *41*, e1900056.
- Orhon, I., Dupont, N., Pampliega, O., Cuervo, A.M., and Codogno, P. (2015). Autophagy and regulation of cilia function and assembly. *Cell Death Differ.* *22*, 389–397.
- Orhon, I., Dupont, N., Zaidan, M., Boitez, V., Burtin, M., Schmitt, A., Capiod, T., Viau, A., Beau, I., Kuehn, E.W., et al. (2016). Primary-cilium-dependent autophagy controls epithelial cell volume in response to fluid flow. *Nat. Cell Biol.* *18*, 657–667.
- Pampliega, O., Orhon, I., Patel, B., Sridhar, S., Díaz-Carretero, A., Beau, I., Codogno, P., Satir, B.H., Satir, P., and Cuervo, A.M. (2013). Functional interaction between autophagy and ciliogenesis. *Nature* *502*, 194–200.
- Phua, S.C., Nihongaki, Y., and Inoue, T. (2018). Autonomy declared by primary cilia through compartmentalization of membrane phosphoinositides. *Curr. Opin. Cell Biol.* *50*, 72–78.
- Reiter, J.F., and Leroux, M.R. (2017). Genes and molecular pathways underpinning ciliopathies. *Nat. Rev. Mol. Cell Biol.* *18*, 533–547.
- Rohatgi, R., Milenkovic, L., and Scott, M.P. (2007). Patched1 regulates hedgehog signaling at the primary cilium. *Science* *317*, 372–376.
- Satir, P., Pedersen, L.B., and Christensen, S.T. (2010). The primary cilium at a glance. *J. Cell Sci.* *123*, 499–503.
- Schink, K.O., Tan, K.-W., and Stenmark, H. (2016). Phosphoinositides in Control of Membrane Dynamics. *Annu. Rev. Cell Dev. Biol.* *32*, 143–171.
- Shewan, A., Eastburn, D.J., and Mostov, K. (2011). Phosphoinositides in cell architecture. *Cold Spring Harb. Perspect. Biol.* *3*, a004796.
- Tang, Z., Lin, M.G., Stowe, T.R., Chen, S., Zhu, M., Stearns, T., Franco, B., and Zhong, Q. (2013). Autophagy promotes primary ciliogenesis by removing OFD1 from centriolar satellites. *Nature* *502*, 254–257.
- Tanida, I., Sou, Y.S., Minematsu-Ikeguchi, N., Ueno, T., and Kominami, E. (2006). Atg8L/Apg8L is the fourth mammalian modifier of mammalian Atg8 conjugation mediated by human Atg4B, Atg7 and Atg3. *FEBS J.* *273*, 2553–2562.
- Wang, L., and Dynlacht, B.D. (2018). The regulation of cilium assembly and disassembly in development and disease. *Development* *145*, dev151407.
- Wheatley, D.N. (1969). Cilia in cell-cultured fibroblasts. I. On their occurrence and relative frequencies in primary cultures and established cell lines. *J. Anat.* *105*, 351–362.
- Wheway, G., Nazlamova, L., and Hancock, J.T. (2018). Signaling through the primary cilium. *Front. Cell Dev. Biol.* *6*, 8.
- Wu, B., and Guo, W. (2015). The Exocyst at a Glance. *J. Cell Sci.* *128*, 2957–2964.
- Xiang, W., Jian, T., Hao, X., Wang, R., Yao, X., Sun, K., Guo, F., and Xu, T. (2019). Primary cilia and autophagy interaction is involved in mechanical stress mediated cartilage development via ERK/mTOR axis. *Life Sci.* *278*, 308–313.
- Xu, C., and Min, J. (2011). Structure and function of WD40 domain proteins. *Protein Cell* *2*, 202–214.
- Xu, Q., Zhang, Y., Wei, Q., Huang, Y., Hu, J., and Ling, K. (2016). Phosphatidylinositol phosphate kinase PIPK1 γ and phosphatase INPP5E coordinate initiation of ciliogenesis. *Nat. Commun.* *7*, 10777.
- Xu, W., Jin, M., Hu, R., Wang, H., Zhang, F., Yuan, S., and Cao, Y. (2017). The Joubert syndrome protein Inpp5e controls ciliogenesis by regulating phosphoinositides at the apical membrane. *J. Am. Soc. Nephrol.* *28*, 118–129.
- Zemirli, N., Boukhalfa, A., Dupont, N., Botti, J., Codogno, P., and Morel, E. (2019). The primary cilium protein folliculin is part of the autophagy signaling pathway to regulate epithelial cell size in response to fluid flow. *Cell Stress* *3*, 100–109.

STAR★METHODS

KEY RESOURCES TABLE

REAGENT or RESOURCE	SOURCE	IDENTIFIER
Antibodies		
Anti-acetylated Tubulin	Sigma	T7451
Anti-actin	Millipore	1501
Anti-ARL13B	Proteintech	66739
Anti-ARL13B	Santa Cruz	515784
Anti-ARL13B	Proteintech	515784
Anti-ATG13	Millipore	MABc46
Anti-ATG16L1	MBL	PM040
Anti-Beclin1	BD Biosciences	612113
Anti-gamma Tubulin	Sigma	T5326
Anti-GFP	Roche	11814460001
Anti-GLI1	Novus	Nb600600
Anti-GM130	BD Biosciences	610823
Anti-GPR161	Sigma	HPA072047
Anti-GST	Sigma	G7781
Anti-IFT20	Proteintech	13615-1-AP
Anti-IFT88	Proteintech	13967
Anti-INPP5E	Proteintech	77797-1-AP
Anti-KIF3A	Proteintech	13930
Anti-LC3B	Sigma	L7543
Anti-mCherry/RFP	Rockland	600401379
Anti-PI4.5P2	Echelon	Z-P045
Anti-PI4P	Echelon	Z-P004
Anti-Sec8	ENZO	814G1
Anti-Sec10	Proteintech	7593-1-AP
Anti-SMO	Abcam	ab38686
Anti-VPS34	ZYMED	382100
Chemicals, peptides, and recombinant proteins		
purmorphamine	Calbiochem	CAS 483367-10-8
Recombinant GST (glutathione-S-transferase)	Fisher Scientific	Cat#15984538
full-length ORF recombinant Human ATG16L1-GST	Creative Biomart	Cat#ATG16L1-945H
Recombinant Human IFT20	Fisher Scientific	Cat#15920229
Critical commercial assays		
Pierce™ GST protein interaction pull-down kit	Fisher Scientific	Cat#21516
Membrane Lipid strip	Echelon	Cat# P-6001
Experimental models: Cell lines		
mouse embryonic fibroblasts (MEFs) CTRL and IFT20 ^{-/-}	Pazour and Cuervo labs	N/A
mouse embryonic fibroblasts (MEFs) CTRL and ATG16L1 ^{-/-}	Tooze lab	N/A
mouse embryonic fibroblasts (MEFs) CTRL and ATG3 ^{-/-}	Mizushima lab	N/A
mouse embryonic fibroblasts (MEFs) CTRL and ATG5 ^{-/-}	Mizushima lab	N/A

(Continued on next page)

Continued

REAGENT or RESOURCE	SOURCE	IDENTIFIER
Human HepG2	ATCC	HB-8065
Oligonucleotides		
oligonucleotides used in this study, see Table S1	N/A	N/A
Recombinant DNA		
RFP-Sec61-beta	T. Rapoport lab	N/A
GFP-ATG16L1	X.M. Yin lab	N/A
mCherry-IFT20	Genecopoeia	A2775

RESOURCE AVAILABILITY

Lead contact

Further information and requests for resources and reagents should be directed to and will be fulfilled by the lead contact, Etienne Morel (Etienne.morel@inserm.fr).

Materials availability

Plasmids and MEFs cell lines generated in this study have not been deposited to any public repository as they are easily generated. Should any of them be needed please inquiry with the lead contact. No other unique reagent was generated in this study.

Data and code availability

This study did not generate/analyze [datasets/codes].

EXPERIMENTAL MODEL AND SUBJECT DETAILS

Cell lines

Mouse Embryonic Fibroblasts (MEFs) Ift20^{-/-} cells were kindly provided by by A.M.Cuervo (Albert Einstein College of Medicine, New York, USA) and were generated by G.J. Pazour (University of Massachusetts, Worcester, Massachusetts, USA). The Atg16L1^{-/-} MEFs were a kind gift from S. Tooze (Francis Crick Institute, London, UK). Atg3^{-/-} and Atg5^{-/-} MEFs were kindly provided by M. Komatsu (Tokyo Metropolitan Institute of Medical Science, Tokyo, Japan) and N. Mizushima (Tokyo Medical and Dental University, Tokyo, Japan) respectively. HEPG2 cells (ATCC) and MEFs were cultured in Dulbecco's Modified Eagle Medium (DMEM), supplemented with 10% FCS or in EBSS (Earle's Balanced Salt Solution) to induce autophagy at 37°C and 5% CO₂.

Cell transfection

The cDNA transfections were performed using lipofectamine 2000 according to the manufacturer's instructions. siRNA transfections were performed using Lipofectamine RNAi Max (Invitrogen, Life Technologies) according to the manufacturer's instructions and two siRNA primers were used for each target at a final concentration of 20nM. All siRNAs were purchased from QIAGEN and the references are as follows: Control siRNA (SI1027281); SEC8 (SI00040894 and SI00040901); RFP-Sec61 β was a kind gift from T. Rapoport (Harvard University, Cambridge, MA, USA). Human GFP-ATG16L1 and IFT20-mcherry constructs were from X.M. Yin (Indianapolis, IN, USA) and Genecopoeia respectively. To generate mutants of GFP-Atg16L1 and mcherry-IFT20, we performed site-directed mutagenesis using a quick change kit (Stratagene), according to the manufacturer's instructions. The sequences of the primers used are specified in the [Key resources table](#).

METHOD DETAILS

Cell treatments

For the serum deprivation experiments, MEFs cells were incubated with DMEM without serum for 24h. When indicated, MEFs were treated by 5 μ m Smoothened (SMO) agonist purmorphamine (Calbiochem) or DMSO under serum deprivation condition during 24 hours.

Protein extraction and western blotting analysis

Cells in 6 wells plates were washed twice with ice-cold PBS and lysed in ice with 200 μ l of 1X Laemmli buffer (60mM Tris-HCL pH = 6.8, 2% SDS, 10% Glycerol, bromophenol blue, supplemented with 100mM DTT) for 30min. Samples were boiled for 10min at 95°C, separated by SDS/PAGE and then transferred onto Nitrocellulose or PVDF membranes. Western blot analysis was performed with specific antibodies and the antigen-antibody complexes were visualized by chemiluminescence (Immobilon Western, Merck Milli-

pore). Secondary HRP conjugate anti-rabbit IgG and HRP conjugate anti-mouse IgG were from GE Healthcare and Bio-Rad, respectively.

In vitro pull-down assay

Interaction between full-length ORF recombinant human ATG16L1-GST (Creative Biomart, Cat#ATG16L1-945H) and recombinant IFT20 (Fisher Scientific Cat#15920229) using pure GST (glutathione-S-transferase, Fisher Scientific, Cat#15984538) as control, was tested with the Pierce™ GST protein interaction pull-down kit (ThermoFisher, Cat#21516) following associated instructions. Briefly, ATG16L1-GST and GST recombinant proteins were dialyzed using Amicon-ULTRA-0.5 10K ultracel devices (Millipore, Cat# UFC501024) to remove excess of glutathione prior to bait preparation. Bait conditions (no protein (empty), ATG16L1-GST or GST) were prepared on glutathione-agarose resin using 4μg of recombinant ATG16L1-Gst or GST alone. For prey capture, bait glutathione-agarose resins were incubated with 4μg recombinant IFT20 protein overnight at 4°C. After extensive wash the bait-prey elution was performed using 10mM glutathione elution buffer (pH 8) and analyzed by western blotting.

Immunofluorescence microscopy and imaging

Cells were fixed either with 4% paraformaldehyde (PFA) for 20min or with cold methanol for 5min at –20°C for proper primary cilium axoneme proteins detection. Cells were then washed and incubated for 30min in blocking buffer (10% FCS or 5% bovine serum albumin in PBS) followed by incubation with primary antibodies diluted in blocking buffer supplemented with 0.05% saponin for 1h at room temperature or overnight at 4°C. Cells were washed 3 times, and then incubated for 1h with fluorescent Alexa Fluor secondary antibodies (donkey anti-sheep IgG, donkey anti-mouse IgG and donkey anti-Rabbit IgG, Life Technologies). Coverslips were mounted with homemade mowiol mounting media. Images were acquired with a Zeiss Apotome.2 fluorescence microscope or Zeiss LSM700 confocal microscope both equipped with 63x oil immersion fluorescence objectives. Number of ciliated cells and length of cilia were quantified using Zen Software (Zeiss).

List of antibodies

Antibody	Catalog Number	WB dilution	IF dilution
Anti-acetylated Tubulin (rabbit)	Sigma-T7451	–	1/500
Anti-actin (mouse)	Millipore-1501	1/10000	–
Anti-ARL13B (mouse)	Proteintech-66739	–	1/200
Anti-ARL13B (mouse)	Santa Cruz-515784	–	1/200
Anti-ARL13B (rabbit)	Proteintech-515784	–	1/500
Anti-ATG13 (mouse)	Millipore-MABc46	–	1/200
Anti-ATG16L1 (rabbit)	MBL-PM040	1/2000	1/200
Anti-Beclin1 (mouse)	BD Biosciences-612113	1/2000	–
Anti-gamma Tubulin (mouse)	Sigma-T5326	–	1/400
Anti-GFP (mouse)	Roche-11814460001	1/5000	–
Anti-GLI1 (mouse)	Novus-Nb600600	1/2000	–
Anti-GM130 (mouse)	BD Biosciences-610823	–	1/500
Anti-GST (rabbit)	Sigma-G7781	1/5000	–
Anti-IFT20 (rabbit)	Proteintech-13615-1-AP	1/1000	–
Anti-GPR161 (rabbit)	Sigma-HPA072047	–	1/400
Anti-IFT88 (rabbit)	Proteintech-13967	–	1/200
Anti-INPP5E (rabbit)	Proteintech-77797-1-AP	1/3000	1/300
Anti-KIF3A (rabbit)	Proteintech-13930	–	1/500
Anti-LC3B (rabbit)	Sigma-L7543	1/10000	–
Anti-mCherry/RFP (rabbit)	ROCKLAND-600401379	1/2000	–
Anti-PI4.5P2 (rabbit)	Echelon-Z-P045	–	1/150
Anti-PI4P (rabbit)	Echelon-Z-P004	–	1/150
Anti-Sec8 (mouse)	ENZO-814G1	1/2500	1/200
Anti-Sec10 (rabbit)	Proteintech-7593-1-AP	1/10000	–
Anti-SMO (goat)	Abcam-ab38686	1/1000	1/400
Anti-VPS34 (rabbit)	ZYMED-382100	1/3000	–

Real time quantitative PCR

RNA was extracted from cells using the NucleoSpin RNA kit (Macherey-Nagel). Reverse transcriptase PCR and qRT-PCR were performed using “Power Sybr green cells to CT” kit (Thermo Fisher Scientific) according to manufacturer’s instructions. Actin was used as reference gene and relative quantification was calculated using the $\Delta\Delta\text{CT}$ method. Primers sequences are described in the [Key resources table](#).

GFP-trap and RFP-trap assays

For immunoprecipitation with GFP-ATG16L1 wt and GFP-ATG16L1 ΔWD40 , MEF ATG16 $^{-/-}$ cells were transiently transfected with plasmids expressing GFP, GFP-ATG16 wt and GFP-ATG16L1 ΔWD40 constructs. For immunoprecipitation with RFP trap, wt IFT20-RFP or YEF1 mutant IFT20 RFP plasmids were transfected in Ift20 $^{-/-}$ or Atg16L1 $^{-/-}$ cells. 24h post transfection, in addition to 24h of complete medium or medium without serum, cells were collected and proteins extracted in lysis buffer (10 mM Tris, pH 7.5, 150 mM NaCl, 0.5 mM EDTA, 0.5% NP-40) complemented with protease and phosphatase inhibitor cocktail (Pierce). Cell lysates were centrifuged at 15,000rpm for 10 min at 4°C. The resulting supernatant was diluted with the dilution buffer (10 mM Tris, pH 7.5, 150 mM NaCl, 0.5mM EDTA) to NP-40final concentration of 0.1%. The protein extracts were incubated with anti-GFP and anti-RFP beads (GFP-Trap Chromotek) for 2 h at 4°C. Beads were collected by centrifugation and washed six times, the protein complexes were eluted by boiling the beads in 1 × SDS-sample buffer for 10 minutes.

Lipid overlay assay

Membrane Lipid strip (Echelon, Cat# P-6001) was used. The human recombinant ATG16L1 (Addgene) was detected on the strips using the protocol stated by the manufacturer. In brief, the strips were blocked using a solution PBS with 3% BSA without fatty acids overnight at 4°C, incubated with the recombinant ATG16L1 or as a positive control the PI4,5P2-GRIP protein 1h at room temperature, washed 6 times for 10 min in washing buffer containing PBS plus 0.1% Tween-20 and detected by chemiluminescence using an anti-rabbit IgG-HRP (Sigma, Spain) or anti GST-HRP antibody (REF) and ECL Detection reagent (Amersham, GE Healthcare, Spain). The concentration of the peptides in the solution was 20 $\mu\text{g/ml}$.

QUANTIFICATION AND STATISTICAL ANALYSIS

Quantification details are described in corresponding figure legends. Data are presented as means \pm SD or SEM. Statistical analyses were performed by unpaired, two-tailed Student’s t test, using GraphPad Prism7 (* $p < 0.005$, ** $p < 0.001$, and *** $p < 0.0001$). Images showing western blotting or immunofluorescence analysis are representative of minimum three independent experiments unless otherwise stated.